Dynamics and properties of waves in a modified Noguchi electrical transmission line

F. B. Pelap,[1,*] J. H. Kamga,[1] S. B. Yamgoue,[2] S. M. Ngounou,[1] and J. E. Ndecfo[1]

[1]*Laboratoire de Mécanique et de Modélisation des Systèmes Physiques, Département de Physique, Université de Dschang, BP 69 Dschang, Cameroun*

[2]*Department of Physics, Higher Teacher Training College Bambili, University of Bamenda, P.O. Box 39 Bamenda, Cameroon*

(Received 21 November 2014; revised manuscript received 14 January 2015; published 27 February 2015)

We consider a modified Noguchi electrical transmission line and examine the effects of a linear capacitance C_s on the wave characteristics while considering the semidiscrete approximation. It appears that wave modulations in the network are governed by a dispersive nonlinear Schrödinger equation whose coefficients are shown to be a function of C_s. We show that the use of this linear capacitance makes the filter more selective. We also show that the width of the unstable regions increases while that of the stable regions decreases with C_s adding consequently the width of the frequency domain where bright solitons exist. Furthermore, we establish the existence of one more region (compared to the work of Marquié *et al.* [Marquié *et al.*, Phys. Rev. E **49**, 828 (1994)]) in the dispersion curve that allows the motion of envelope solitons of higher frequency in the system. Numerical and experimental investigations done on the model confirm our analytical predictions.

DOI: 10.1103/PhysRevE.91.022925 PACS number(s): 05.45.Yv, 05.50.+q, 05.90.+m

I. INTRODUCTION

Nonlinear transmission lines (NLTLs) are known as convenient tools to study wave propagation in nonlinear dispersive media. Since the pioneering work by Hirota and Suzuki [1] on electrical lines simulating Toda lattices [2], growing interest has been devoted to the use of NLTLs, in particular for the study of nonlinear wave propagation [3–10]. This great amount of attention is motivated by the capacity of these lines to support soliton excitations [11,12] and because they provide a useful way to model the exotic properties of new systems [13–15].

Contributing to the understanding of this mechanism is the motivation of this paper. Indeed, Noguchi built a new type of electrical transmission line to study experimentally the propagation of the first-order Korteweg–de Vries (KdV) solitons [16]. This line was different from the Hirota-Suzuki model [1] by the presence of a linear dispersive capacitance C_s. This network was exploited to carry out theoretical investigations of the motion of the second-order KdV solitons using the Toda potential [17]. Moreover, Yoshinaga and Kakutani considered this Noguchi line and examined experimentally the properties of the second-order KdV solitons using a new potential that generalized the Toda potential [18]. Unfortunately, it clearly appears that all these studies on the Noguchi's electrical transmission line neglect the effects of C_s.

In this work we introduce a modified version of Noguchi's model and examine the effects of the linear capacitance C_s on the wave characteristics and their consequences on existing research works. This paper is organized as follows. In Sec. II a brief description of the model is given and the basic equations of the modified discrete Noguchi transmission line are presented. In the limit of small wave amplitudes, the linear dispersion law is derived and the impact of C_s is found. In Sec. III we consider the semidiscrete approximation and establish that the dynamics of modulated waves is described by a dispersive nonlinear Schrödinger equation (DNLSE). The effects of the linear capacitance are investigated in terms of both the modulational instability occurrence and the nature of the corresponding soliton solutions of the DNLSE. In Sec. IV we present the contribution of the dc term in the general solution of the circuit equations. Indeed, this term was not taken into account in the work of Marquié *et al.* [6]. Analytical results are established. These results are completed by numerical and experimental studies performed in the network. Section V is devoted to a summary and discussion.

II. MODEL DESCRIPTION AND BASIC EQUATIONS

Our model is a lossless one-dimensional modified discrete Noguchi electrical transmission line (Fig. 1) made of N identical unit cells. Each unit cell is modeled by a linear inductor L_1 in parallel with a linear capacitance C_s in the series branch and a linear inductance L_2 in parallel with a nonlinear capacitor $C(V)$ in the shunt branches. In this line, the nonlinear capacitance consists of a reversed biased diode with differential capacitance function of the voltage V_n across the nth capacitor and biased by a constant voltage V_0: $C(V_0+V_n)=dQ_n/dV_n$, where $Q_n(V_n)$ is the corresponding nonlinear charge. For low voltages taken around V_0, the quantity $Q_n(V_n)$ can be approximated by [19]

$$Q_n(V_n)\approx C_0\left(V_n-\alpha V_n^2+\beta V_n^3\right), \tag{1}$$

where $C_0=C(V_0)$ is the characteristic capacitance and α and β are nonlinear positive constants.

By applying the Kirchhoff laws to the circuit of Fig. 1, we obtain the following system of equations that describe the propagation of the voltage $V_n(t)$ in the network:

$$\begin{aligned}&\frac{d^2V_n}{dt^2}+u_0^2(2V_n-V_{n-1}-V_{n+1})\\&\quad+\lambda\frac{d^2}{dt^2}(2V_n-V_{n-1}-V_{n+1})+\omega_0^2V_n\\&\quad=\alpha\frac{d^2V_n^2}{dt^2}-\beta\frac{d^2V_n^3}{dt^2},\quad n=1,2,\ldots,N,\end{aligned} \tag{2}$$

where $u_0^2=1/L_1C_0$, $\lambda=C_s/C_0$, $\omega_0^2=1/L_2C_0$, and N is the number of cells considered. In the following, we plan to solve

*Corresponding author: fbpelap@yahoo.fr

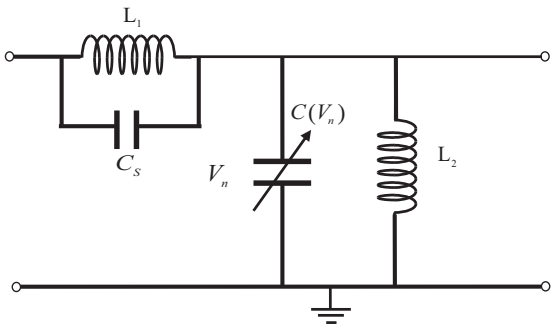

FIG. 1. Schematic representation of one unit cell of a modified discrete Noguchi electrical transmission line. The network possesses N identical unit cells.

Eq. (2) for non-null values of λ and present the impact of the additional dispersion (introduced by C_s) on the characteristic parameters of the signal. Numerical investigations are made for the following values of the network parameters:

$$L_1 = 220\ \mu\text{H}, \quad L_2 = 470\ \mu\text{H}, \quad V_0 = 2\ \text{V}, \quad C_0 = 320\ \text{pF},$$
$$\alpha = 0.21\ \text{V}^{-1}, \quad \beta = 0.0197\ \text{V}^{-2}, \quad C_S = 56\ \text{pF} \qquad (3)$$

It should be stressed that these parameters are not chosen arbitrarily [6]. Indeed, the linear capacitance C_s is regarded as the stray capacitance mainly due to the interwire capacitance of the inductor L_1 whose effects are not neglected in this work. Therefore, in practice we should always have $C_s \ll C_0$ [18,20,21] so that the ratio $\lambda = C_0/C_s$ will always remains less than the unit. The normalized capacitance λ represents an additional dispersion.

Linear oscillations in the line with wave number k and frequency ω are governed by the following linear dispersion law:

$$\omega^2 = \left[\omega_0^2 + 4u_0^2 \sin^2(k/2)\right]/[1 + 4\lambda \sin^2(k/2)]. \qquad (4)$$

For values of k chosen in the first Brillouin zone ($0 \leqslant k \leqslant \pi$), the curves of Fig. 2 show the dependence of the frequency $f = \omega/2\pi$ as a function of k for different values of the linear term λ and represent a bandpass filter. As displayed on these plots, the corresponding linear spectrum has a gap $f_0 = \omega_0/2\pi$, which is the lower cutoff frequency introduced by the parallel inductance L_2, and it is limited by the cutoff frequency

$$f_{\max} = \frac{\omega_{\max}}{2\pi} = \frac{1}{2\pi}\sqrt{\left(\omega_0^2 + 4u_0^2\right)/(1 + 4\lambda)} \qquad (5)$$

due to the intrinsic discrete character of the lattice. This cutoff frequency $f_{\max}$ decreases with the growth of λ, which means that the linear dispersion λ contributes to reduce the network effects on the wave during its motion. These results also mean that the frequency bandpass of the modified Noguchi filter decreases with values of λ and becomes more selective in terms of frequency. We could also note that the upper gap zone increases for nonzero values of C_s. Therefore, the model is also appropriate for the investigation of upper gap soliton dynamics. Hereafter, we will focus our attention on the nonlinear behavior of the lattice.

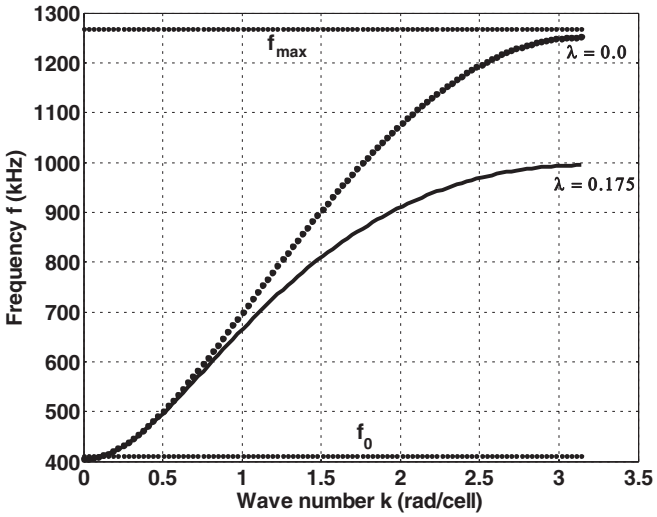

FIG. 2. Linear dispersive curve showing evolution of the frequency $f = \omega/2\pi$ as a function of the wave number k for given values of λ. This curve is constructed for the following line parameters defined by Eqs. (3). The lower cutoff frequency is $f_0 = 411$ kHz. The upper cutoff frequencies are, respectively, $f_{\max} = 1268$ kHz for $\lambda = 0$ and $f_{\max} = 972.5$ kHz for $\lambda = 0.175$. We note that the frequency domain $[f_0, f_{\max}]$ of the filter decreases with the growth of λ and the filter becomes more selective.

III. MODULATED WAVES AND THE DISPERSIVE NONLINEAR SCHRÖDINGER EQUATION

Now we focus our attention on the propagation of modulated waves in the system. Therefore, to derive the amplitude equation describing the motion of such waves, we make the following statements.

(i) We consider the reductive perturbation approach in the semidiscrete approximation [22] to obtain short-wavelength envelope solitons. This approach allows us to treat properly the carrier with its discrete character and to describe the envelope in the continuum approximation. Here new space and time variables (X,T) are introduced related to the basic ones (n,t) through a parameter ε that measures the smallness of the modulation frequency and the amplitude of the input waves:

$$X = \varepsilon(n - V_g t), \quad T = \varepsilon^2 t. \qquad (6)$$

It becomes possible to separate fast and slow variations of V_n in both space and time by setting that V_n depends not only on n and t but also on X and T, i.e., $V_n(t) = V(n,t,X,T)$. In Eq. (6) the quantity V_g designates the group velocity of the linear wave packets given below and plotted (Fig. 3) as a function of the wave number k for different values of λ:

$$V_g = \frac{\partial \omega}{\partial k} = \left[\left(u_0^2 - \lambda\omega^2\right)\sin k\right]/\{\omega[1 + 4\lambda \sin^2(k/2)]\}. \qquad (7)$$

The obtained curves show that the velocity of a wave packet decreases as the value of the parameter λ increases, suggesting that the wave packet will spend more time in the network for nonzero values of λ.

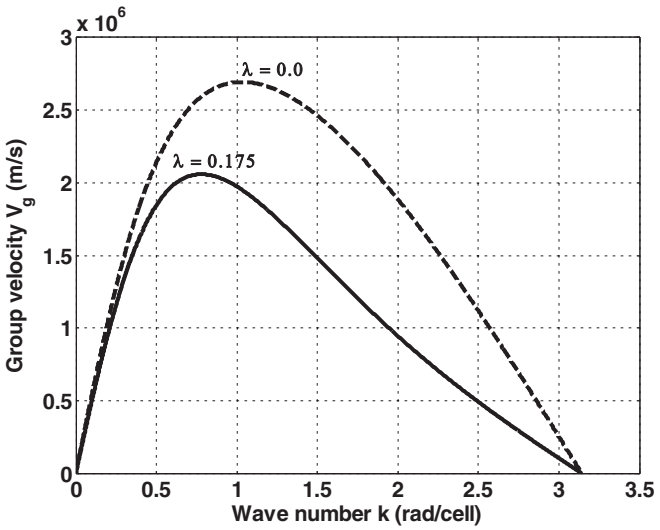

FIG. 3. Group velocity V_g versus k for the line parameters of Fig. 2. This velocity decreases when λ increases. This result suggests that a wave packet moving in the network will travel for a long distance before it vanishes.

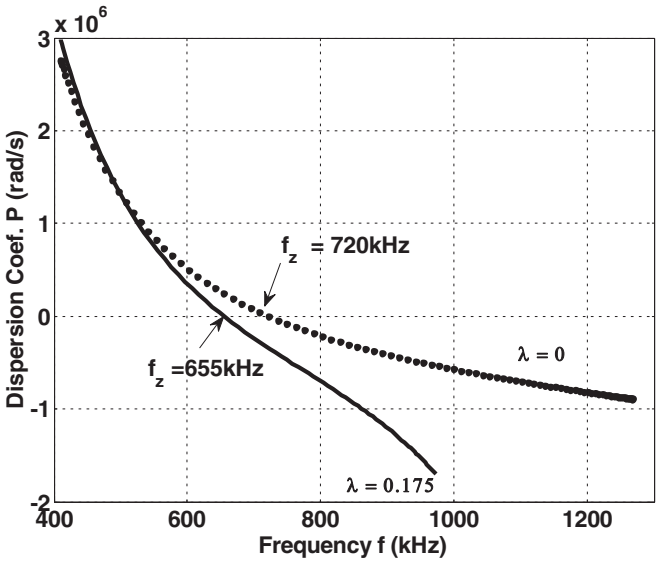

FIG. 4. Behavior of the dispersive coefficient P as a function of the frequency of the carrier f for different values of λ and the line parameters of Fig. 2. These curves show that P vanishes for a frequency f_z whose value decreases with the growth of λ.

(ii) The general oscillating solution for the voltage $V_n(t)$ is assumed to have the following form:

$$V_n(t) = \varepsilon V_1(X,T)e^{i\theta(n,t)} + \text{c.c.} + \varepsilon^2 V_{20}(X,T) + \varepsilon^2 V_2(X,T)e^{2i\theta(n,t)} + \text{c.c.}, \quad (8)$$

in which $\theta = nk - \omega t$ is the rapidly varying phase and c.c. stands for the complex conjugation. The dc and second-harmonic terms $V_{20}(X,T)$ and $V_2(X,T)$, respectively, are added to the fundamental one $V_1(X,T)$ in order to take into account the asymmetry of the charge-voltage relation given by Eq. (1). In spite of the bandpass character of our filter, we will consider the solution (8) in its complete form and appreciate the contribution of the dc term.

(iii) During the computations, there are also nonzero voltages $V_l(n \pm 1,t)$, which are expanded in the continuum limit around $V_l(X,T)$ with $n = X$. So fast changes of the phase θ in Eq. (6) are correctly taken into account by considering differences in the phase for the discrete variable n. Since we are interested only in modulated waves with a slowly varying envelope in space and time, we scale time and space derivatives as $\partial/\partial t \sim O(\varepsilon)$ and $\partial/\partial x \sim O(\varepsilon)$, respectively, and neglect consistently ε terms of high order. Then we keep derivative terms of $V_n(t)$ up to second order to balance dispersion and nonlinearity.

With the above considerations, the substitution of $V_n(t)$ and its derivatives into Eq. (2) leads, for the terms proportional to $\varepsilon^3 e^{i\theta}$, to the DNLSE

$$iV_{1,T} + PV_{1,XX} + Q|V_1|^2 V_1 = 0 \quad (9)$$

in which the dispersive and the nonlinear coefficients (P, Q) are, respectively, defined by

$$P = -\frac{V_g^2}{2\omega}\left(1 + 4\lambda\sin^2\frac{k}{2}\right) + \left(\frac{u_0^2}{2\omega} - \frac{\lambda\omega}{2}\right)\cos k - 2\lambda V_g \sin k, \quad (10)$$

$$Q = M_{22} + M_{21} + M_{23} \quad \text{for} \quad M_{21} = -\alpha^2\omega^3/D_0, \quad M_{22} = 3\beta\omega/2, \quad (11)$$

$$D_0 = \omega^2 + \left(4\lambda\omega^2 - u_0^2\right)\sin^2 k - \tfrac{1}{4}\omega_0^2, \quad M_{23} = -2\alpha^2\omega V_g^2/\left(V_g^2 - u_0^2\right). \quad (12)$$

Moreover, we show that the continuous component $V_{20}(X,T)$ of the voltage as well as its second harmonic $V_2(X,T)$, respectively obtained for terms proportional to $\varepsilon^4 e^{0i\theta}$ and $\varepsilon^2 e^{2i\theta}$, are connected to the fundamental V_1 by the following relations:

$$V_{20} = -(M_{23}/\alpha)|V_1|^2, \quad V_2 = (\alpha\omega^2/D_0)(V_1)^2. \quad (13)$$

Relations (13) show that the nonlinear coefficients M_{23} and M_{21} come from the contribution of $V_{20}(X,T)$ and $V_2(X,T)$, respectively. It appears from expressions (10) and (11) that P and Q depend on the linear term λ as illustrated in Figs. 4 and 5. This allows us to refer to relation (9) as the DNLSE. Figure 4 indicates that the dispersion coefficient P vanishes for a value of the wave number k_z that corresponds to the frequency $f_z = 720$ kHz for $\lambda = 0$. In the case $\lambda = 0.175$, this frequency is reduced to $f_z = 655$ kHz. As far as the behavior of the nonlinear coefficient Q is concerned, we observe that its maximum value decreases when values of λ grow (Fig. 5). We have noted that Q vanishes for frequencies f_q and f_Q to be determined. The values of these frequencies are also reduced for $\lambda = 0.175$.

Furthermore, we investigate the behavior of the product PQ as a function of the wave number k for different values of the additional linear dispersion λ (Fig. 6). Since the DNLSE (9) keeps the same form in the absence of λ, the modulational instability (MI) criterion established by Benjamen and Feir [23] remains valid, but critical values of

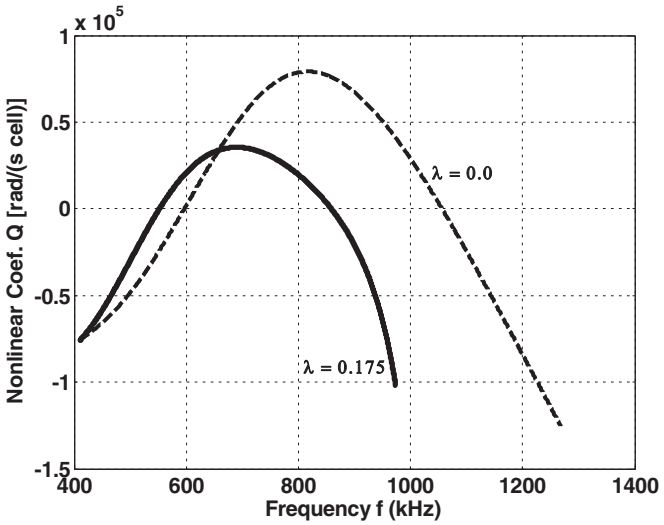

FIG. 5. Plot of the nonlinear coefficient Q in terms of f for the parameters of Fig. 2. We note that the maximum value of Q passes from 7.92×10^4 rad/s V for $\lambda = 0$ to the value 3.575×10^4 rad/s V for $\lambda = 0.175$.

k at the marginal state ($PQ \approx 0$) change in the presence of λ (Fig. 6). However, a uniform wave train propagating along the modified Noguchi electrical transmission line will become unstable under the modulation for $PQ > 0$ and will remain stable for $PQ < 0$. According to Fig. 6, points $A1$, $B1$, and $C1$ are zeros of PQ for $\lambda = 0$ while $A2$, $B2$, and $C2$ are its zeros for $\lambda = 0.175$. Therefore, we introduce the quantities

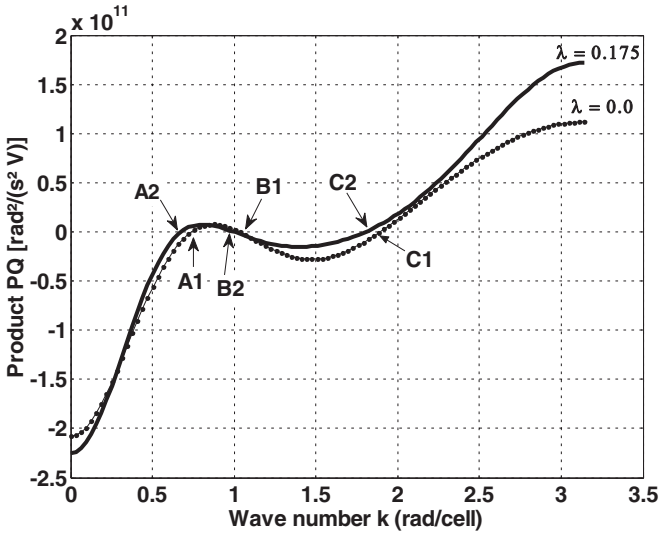

FIG. 6. Variations of the product PQ as a function of k for given values of λ. Points $A1$ ($k_{A1} = 0.74$), $B1$ ($k_{B1} = 1.04$), and $C1$ ($k_{C1} = 1.89$) are zeros of PQ for $\lambda = 0$, while this product vanishes at $A2$ ($k_{A2} = 0.68$), $B2$ ($k_{B2} = 1$), and $C2$ ($k_{C2} = 1.80$) for $\lambda = 0.175$. We define the quantities $z_1 = k_{B1} - k_{A1} = 0.3$, $z_2 = k_{B2} - k_{A2} = 0.32$, $z_3 = k_{C1} - k_{B1} = 0.85$, and $z_4 = k_{C2} - k_{B2} = 0.8$. Since $z_2 > z_1$, the modulational instability zone increases when λ grows. On the other hand, we have $z_4 < z_3$, which implies that the modulational stability zone decreases with λ. In both cases, we note that the curve can be divided into four regions that deal with the signs of PQ.

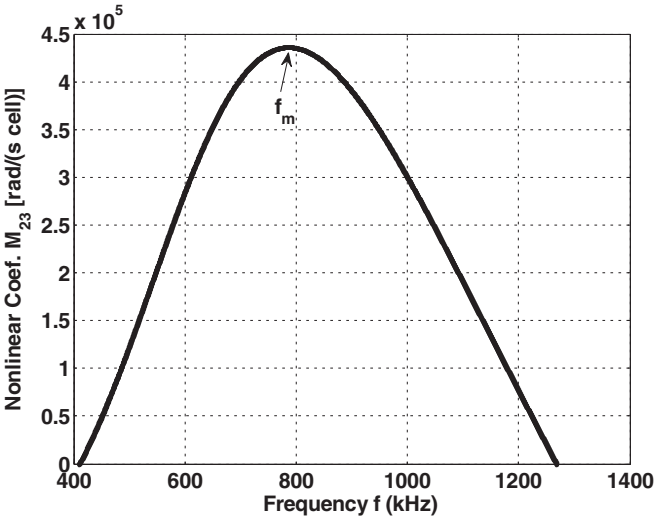

FIG. 7. Behavior of the nonlinear coefficient M_{23} versus the frequency f of the carrier for the line parameters of Fig. 2 in the case $\lambda = 0$. This curve shows that M_{23} does not possess neglected values in spite of the bandpass character of our filter and also establishes the existence of a maximum value at $f_m = 789.4$ kHz.

$z_1 = k_{B1} - k_{A1} = 0.3$, $z_2 = k_{B2} - k_{A2} = 0.32$, $z_3 = k_{C1} - k_{B1} = 0.85$, and $z_4 = k_{C2} - k_{B2} = 0.8$. Since $z_2 > z_1$, the MI zone increases when λ grows. On the other hand, we have $z_4 < z_3$, which implies that the modulational stability zone decreases with λ. In both cases, we note that the curve can be divided into four regions that deal with the signs of PQ. These results suggest that the behavior of the product PQ should be checked in terms of the frequency to establish clearly the limits of each region. Based on the results already established on the cubic nonlinear Schrödinger (NLS) equation [4,24], the DNLS equation (9) will have both a dark soliton (for $PQ < 0$) and a bright soliton (for $PQ > 0$).

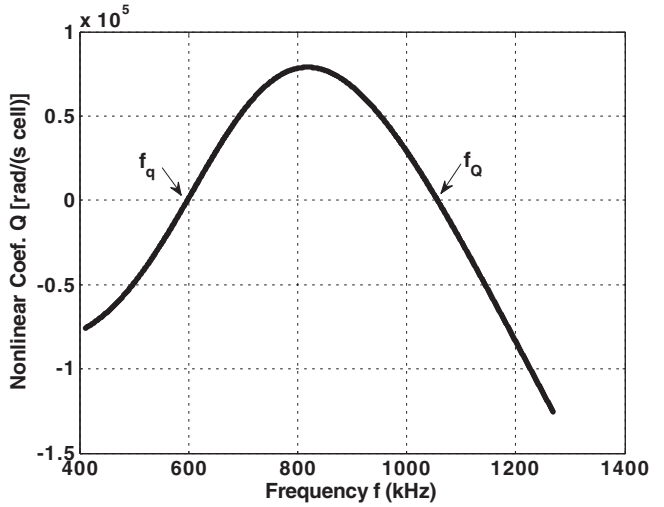

FIG. 8. Evolution of the nonlinear coefficient Q in terms of the frequency f for the parameters of Fig. 2 in the case $\lambda = 0$. We note that nonlinear effects vanish for two values of the frequency $f_q = 590$ kHz and $f_Q = 1062$ kHz. The second frequency f_Q was absent in many works carried out on this bandpass filter [6,25–27].

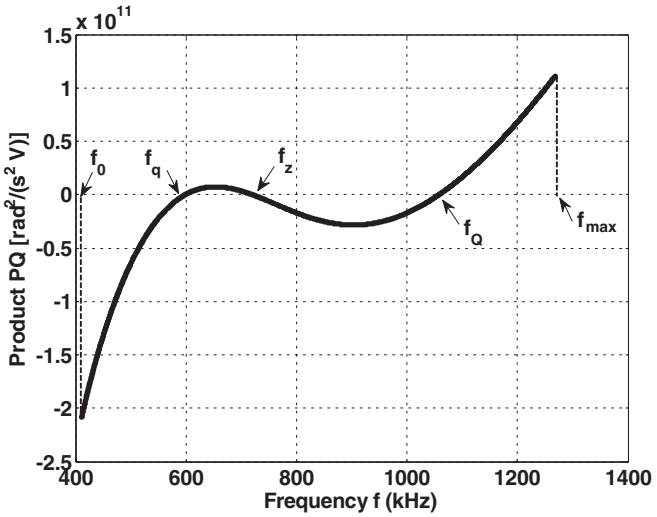

FIG. 9. Variations of the product PQ as a function of the frequency f for the parameters of Fig. 2 with $\lambda = 0$. We obtain three characteristic frequencies where this product vanishes, that is, $f_q = 590$ kHz, $f_z = 720$ kHz, and $f_Q = 1062$ kHz, which divide the curve into four regions that deal with the signs of PQ.

On the other hand, we mentioned above that the curve of PQ as a function of k can be divided into four regions. It should be stressed that previous works [6,25–27] on this bandpass filter (model without C_S) divided this curve in only three regions. In the following section we intend to emphasize this difference.

IV. CONTRIBUTION OF THE dc TERM

In this section we establish the contribution of the dc term $V_{20}(X,T)$ as part of the general modulated solution $V_n(t)$ of the circuit equations [Eq. (2) with $\lambda = 0$] in the semidiscrete approximation. Our investigation is motivated by the fact that in one of their papers [6], Marquié *et al.* assume that "the dc term $V_{20}(X,T)$ will vanish due to the existence of the low-frequency forbidden band in the dispersion curve." This assertion could have great impact on the wave equation and the instability domains. Hereafter, we plan to appreciate the influence of this term on these different named quantities. To achieve this aim, we will follow our finding in the case $\lambda = 0$.

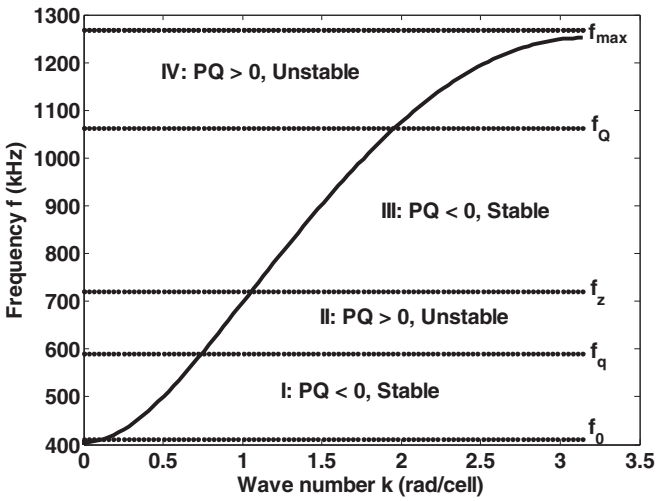

FIG. 10. Dispersion curve of our bandpass filter in the case $\lambda = 0$. The allowed band $[f_0, f_{\max}]$ is divided into four regions concerning the stability of the system, which depends on the sign of the product PQ. Previous works [6,25–27] exhibit only three domains of frequency.

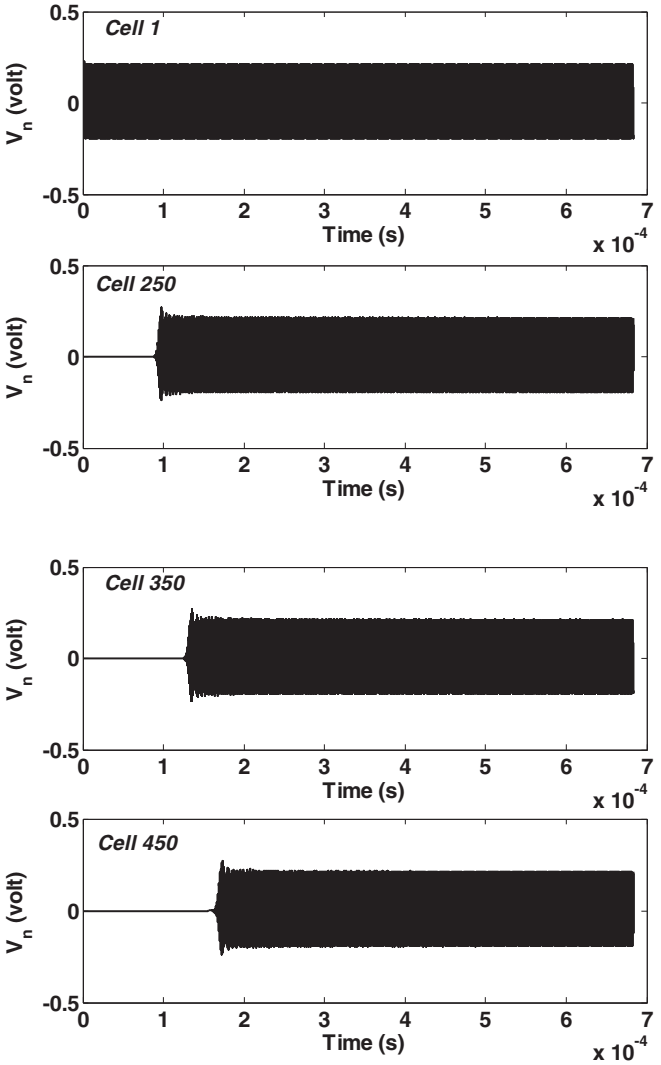

FIG. 11. Signal voltage as a function of time showing stability of the plane wave at frequency $f_P = 460$ kHz belonging to domain I of the dispersion curve. The initial amplitude $V_m = 0.2$ V, while the modulation rate $b = 1\%$ and modulation frequency $f_m = 8.75$ kHz.

A. Nonlinear coefficient Q

Now we focus our attention on the contribution of the dc term $V_{20}(X,T)$ on the nonlinear coefficient Q. For this purpose, considering the case $\lambda = 0$, we obtain from Eqs. (4) and (10) that the dispersion law and the dispersion coefficient are respectively defined by

$$\omega^2 = \omega_0^2 + 4u_0^2 \sin^2(k/2), \tag{14}$$

$$P = \left(u_0^2 \cos k - V_g^2\right)/2\omega = P_0. \tag{15}$$

Based on relation (14), it is easy to show that

$$M_{22}+M_{21}=\omega\left[\frac{3\beta}{2}-\frac{4\alpha^2\left[\omega_0^2+4u_0^2\sin^2(k/2)\right]}{3\omega_0^2+16u_0^2\sin^4(k/2)}\right]=Q_0. \tag{16}$$

Therefore, we can write expression (11) in the simplest form

$$Q=Q_0+M_{23}. \tag{17}$$

In relations (15) and (17), the quantities P_0 and Q_0 represent, respectively, the dispersion and nonlinear coefficients obtained by Marquie *et al.* [6]. It should be stressed that we have the same expression of P_0, but our Q is defined by Eq. (17), in which the additional term M_{23} comes from the presence of the dc term $V_{20}(X,T)$ within the solution $V_n(t)$. To measure the contribution of this nonlinear coefficient M_{23}, we seek its behavior in terms of the frequency f of the carrier (Fig. 7). This plot shows that M_{23} presents a maximum value at $f_m=789.4$ kHz. It also appears from this graph that the contribution of M_{23} cannot be neglected in either the lower or upper frequency. Thus it becomes impossible to ignore its impact on the nonlinear coefficient. On the other hand, we observe that (Fig. 8) evolution of Q exhibits a parabolic behavior as a function of the frequency f with a maximum value at $F_m=816$ kHz. This curve shows that the nonlinear coefficient Q vanishes for two values of the frequency, namely, $f_q=590$ kHz and $f_Q=1062$ kHz. The latter frequency was absent in the study of Marquié *et al.* [6]. Its presence is justified by the existence of M_{23}. In the following we check the consequence of the appearance of f_Q on the behavior of the product PQ.

B. Product *PQ*

By considering expressions (15) and (17), we examine the evolution of the product PQ as a function of the frequency f of the carrier (Fig. 9). This plot establishes that the product PQ is null for three values of the frequency, namely, $f_q=590$ kHz, $f_z=720$ kHz, and $f_Q=1062$ kHz. Let us recall

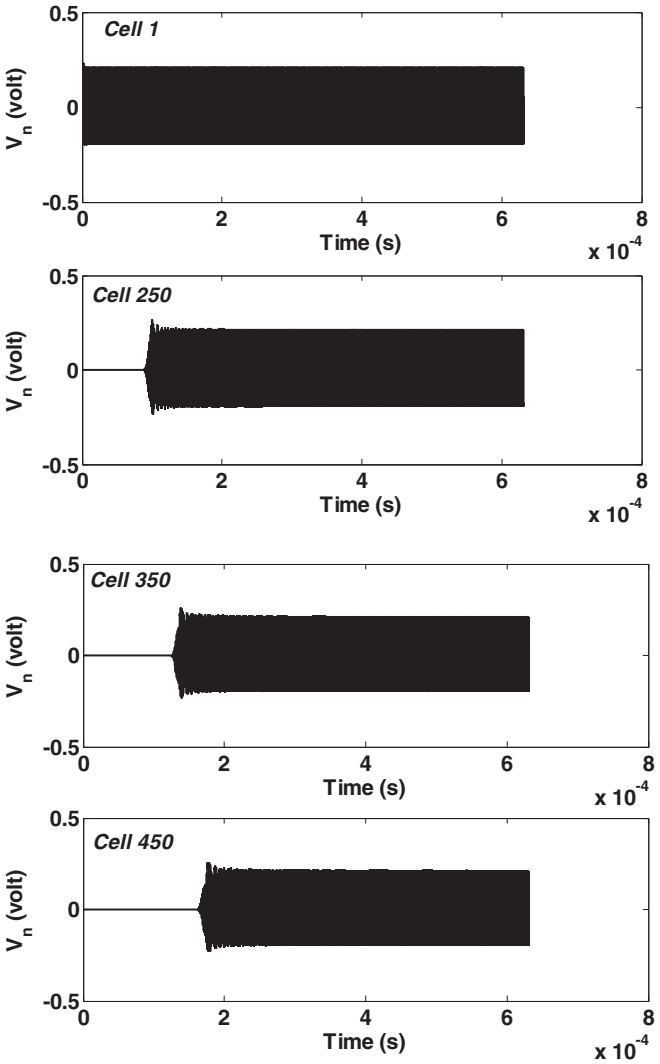

FIG. 12. Signal voltage versus time exhibiting the stability of the plane wave for the frequency $f_p=810$ kHz (domain III) with the parameters of Fig. 11.

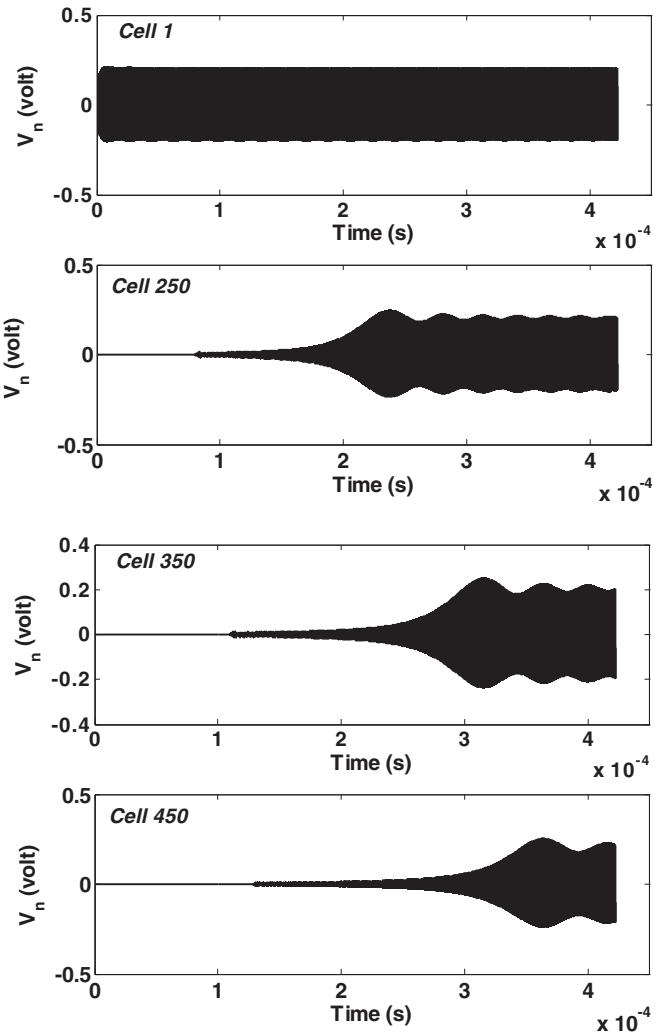

FIG. 13. Modulational instability phenomenon of the plane wave for the frequency $f_p=622$ kHz that belongs to domain II of the dispersion curve with the parameters of Fig. 11.

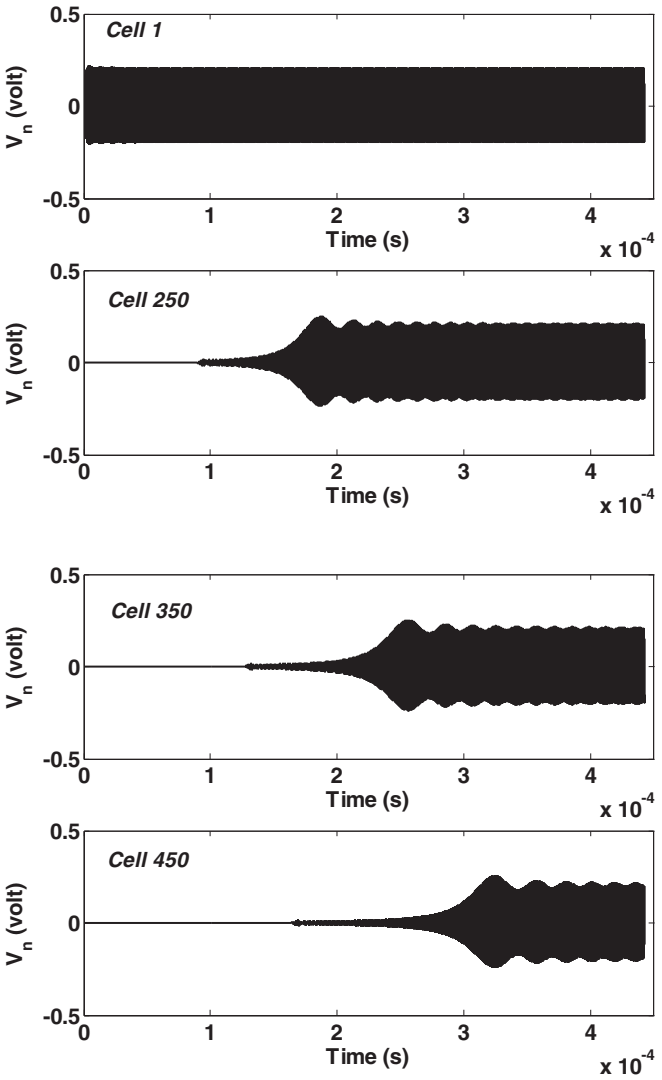

FIG. 14. Modulational instability phenomenon of the plane wave observed at the frequency $f_p = 1205$ kHz that belongs to region IV with the parameters of Fig. 11.

that f_z corresponds to the zero of the dispersion coefficient P, while f_q and f_Q are zeros of the nonlinear coefficient Q.

According to Benjamin and Feir's instability criterion [23], Fig. 9 establishes the existence of four regions concerning the modulational instability of the plane wave and possible soliton solutions of the wave equation [4,24].

Region I. The parameters are $f \in [f_0, f_q]$, $P > 0$, $Q < 0$, and $PQ < 0$, with modulational stability and a hole soliton.

Region II. The parameters are $f \in [f_q, f_z]$, $P > 0$, $Q > 0$, and $PQ > 0$, with modulational instability and an envelope soliton.

Region III. The parameters are $f \in [f_z, f_Q]$, $P < 0$, $Q > 0$, and $PQ < 0$, with modulational stability and a hole soliton.

Region IV. The parameters are $f \in [f_Q, f_{\max}]$, $P < 0$, $Q < 0$, and $PQ > 0$, with modulational instability and an envelope soliton.

Let us summarize those results on the dispersion relation curve as given by Fig. 10. As we can observe from this figure, the curve presents four regions depending on the sign of PQ instead of three regions as shown in Refs. [6,25–27].

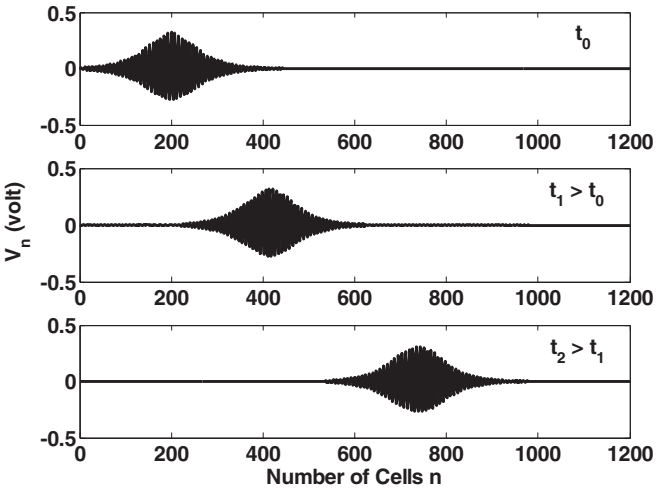

FIG. 15. Propagation of the bright soliton solution of the NLS equation in the network for $f_p = 622$ kHz with the initial amplitude $V_m = 0.3$ V.

C. Numerical investigations

The main purpose of this section is to present the results of numerical simulations performed on the exact discrete equation (2) governing the wave propagation in the nonlinear electrical network. Therefore, integration of the equations of motion (2) is done through the fourth-order Runge-Kutta method. Our analysis is carried out on a discrete electrical transmission line (Fig. 1) made of 1200 cells and fixed boundary conditions. The parameters of the network are those of Sec. II and the linear dispersion factor $\lambda = 0.0$. We will examine numerically the modulational instability phenomenon and the propagation of the envelope soliton in the line.

1. Asymptotic behavior of plane waves

According to the analytical results presented in Sec. IV B, a plane wave introduced in the network becomes unstable when $PQ > 0$ and remains stable for $PQ < 0$. To numerically achieve

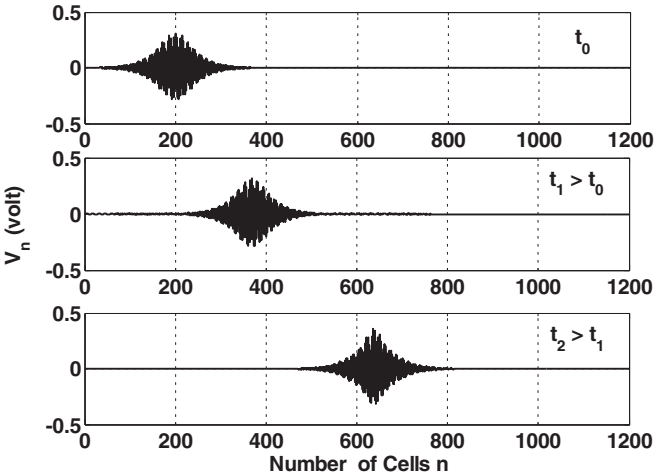

FIG. 16. Transmission of the bright soliton solution of the NLS equation through the network for $f_p = 1205$ kHz and $V_m = 0.3$ V.

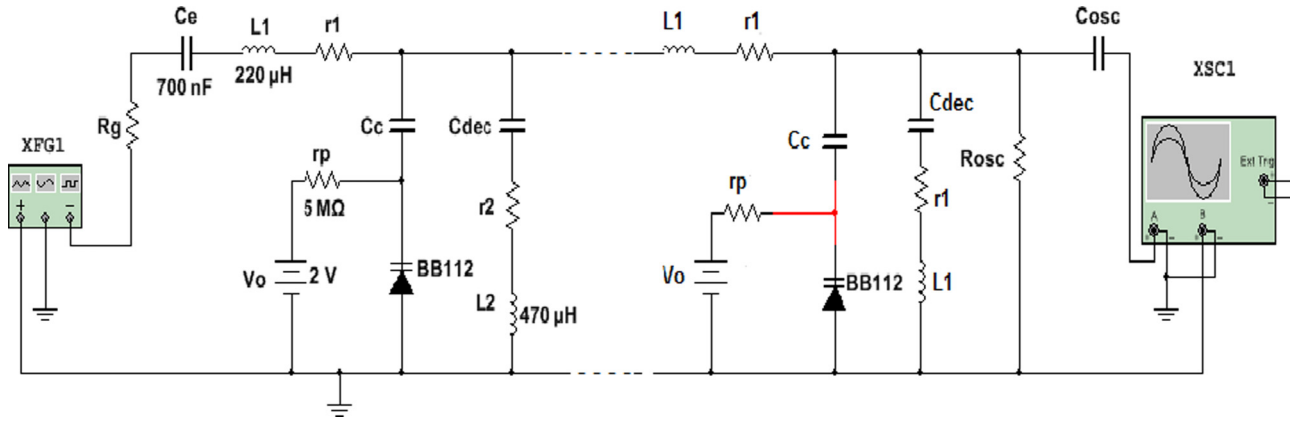

FIG. 17. (Color online) Schematic representation of the experimental arrangement.

this aim, the following signal is applied at the input of the line:

$$V_e(t) = V_m(1 + b\cos\omega_m t)\cos\omega_p t. \tag{18}$$

In this relation, V_m designates the amplitude of the unperturbed plane wave with angular frequency $\omega_p = 2\pi f_p$ and b and $\omega_m = 2\pi f_m$ stand, respectively, for the rate and the angular frequency of the modulation. Investigations of the asymptotic behavior of plane waves are made over the whole carrier wave frequency range $f_0 < f_p < f_{\max}$ and for modulation frequencies $0.1 < f_m < 10$ kHz. The parameters of the input signal are, respectively, $V_m = 0.2$ V, $f_m = 8.75$ kHz, and $b = 1\%$ and the cells 1, 250, 350, and 450 are arbitrary chosen to observe the behavior of the input signal during its propagation in the network.

Based on the results summarized in Fig. 10, the plane wave injected in the line will remain stable under the modulation for $f_p \in [f_0, f_q]$ and $f_p \in [f_z, f_Q]$, which link domains I and III, respectively. When the carrier wave frequencies are taken to be $f_P = 460$ and 810 kHz, we obtain the results plotted, respectively, in Figs. 11 and 12, showing the stability of the plane wave after its adaptation in the line. On the other hand, the results of Fig. 10 show that any plane wave introduced in the line is supposed to be modulationally unstable for $f_p \in [f_q, f_z]$ and $f_p \in [f_Q, f_{\max}]$, which deals with domains II and IV, respectively. For the frequencies $f_p = 622$ and 1205 kHz, the graphs of Figs. 13 and 14 exhibit the behavior of a plane wave in the system. We note that as time increases, the wave that travels in the network breaks into a periodic pulse train leading to its self-modulation. At the end, we observe that numerical analysis yields results that agree with our analytical predictions summarized in Fig. 10.

2. *Propagation of envelope solitons*

To experience the transmission of the envelope soliton through our model for several bands of frequencies dictated by Fig. 10, we excite one extremity of the line with an envelope solution of the NLS equation [6]. In order to avoid signal reflection that disturbs the accurate observation of the wave propagation in the network, the voltage across the other extremity is set to zero and the experiment is run for a sufficiently long time. The results of the numerical simulations are given in Figs. 15 and 16. These curves present the spatial evolution of the envelope solution for given time t_0, t_1, and t_2. It appears that data can be carried out through the nonlinear transmission line of Fig. 1 without major distortion.

D. Experimental studies

The NLTL under consideration (Fig. 17) is implemented and simulated by means of the NI Multisim software using realistic components for circuit simulations. The network is made of 16 identical cells in which each diode BB112 is biased by $V_0 = 2$ V through a resistance of $R = 5$ MΩ. Linear capacitors C_c, C_{dec}, and C_{osc} are used to block the

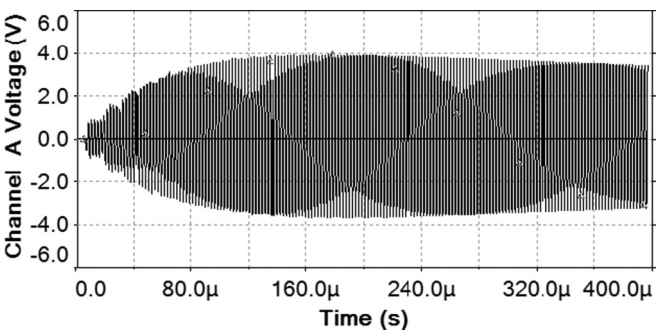

FIG. 18. Experimental stability of the plane wave with the frequency $f_p = 460$ kHz belonging to region I of the dispersion curve (Fig. 10) observed in cell 16.

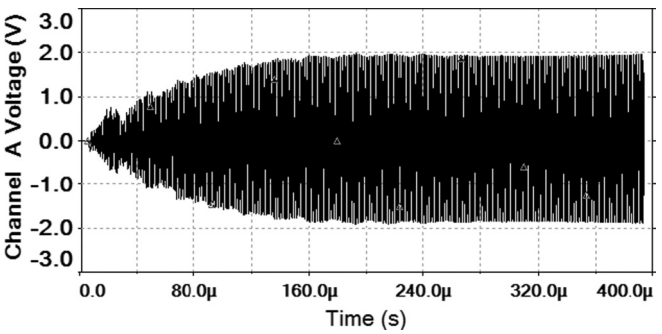

FIG. 19. Experimental stability of the signal with a carrier wave frequency chosen in domain III ($f_p = 810$ kHz) with the parameter of Fig. 18.

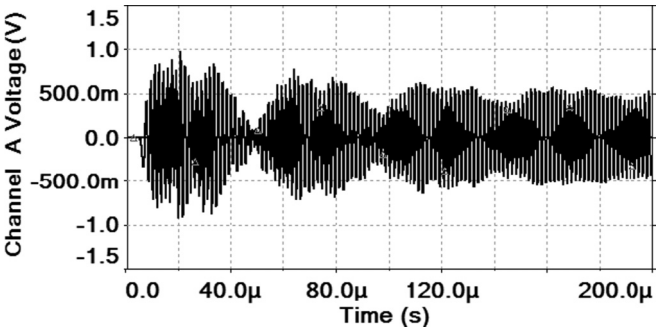

FIG. 20. Experimental observation of the instability under modulation of the plane wave at frequency $f_p = 622$ kHz belonging to domain II of the dispersion curve where $PQ > 0$. The signal is at cell 16.

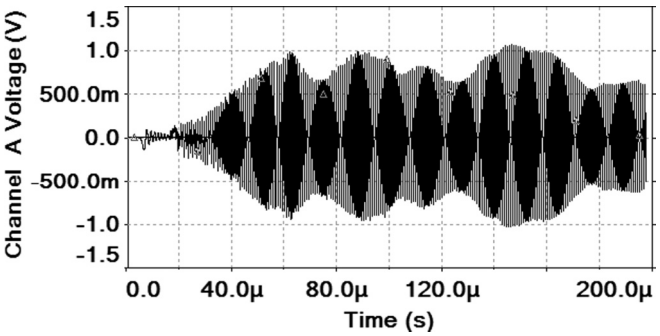

FIG. 21. Experimental observation of the MI phenomenon of the signal of frequency $f_p = 1205$ kHz belonging to domain IV of the dispersion curve with the parameter of Fig. 20.

dc biased current but have no effects on the considered frequencies range. The linear resistor R_g is also introduced to protect the programmable generator XFG1. The linear inductors $L_1 = 220$ μH and $L_2 = 470$ μH possess associated resistances of r_1 and r_2, respectively.

The waves are created in the programmable generator and the waveforms are observed and stored in the numerical oscilloscope XSC1, which has high impedance used to avoid signal reflection**.** Experimental results are given for the modulational stability or instability of a plane wave that propagates in the system. This wave dynamics is observed in cell 21. According to Fig. 10, for the choice of the carried frequencies $f_P = 460$ and 810 kHz that belong to the stability regions I and III, respectively, the plots of Figs. 18 and 19 present the behavior of the plane wave in the experimental line. It appears from those graphs that after a slide adaptation to the line, the wave propagates in the network without modulation.

On the other hand, for frequencies $f_p = 622$ and 1205 kHz taken, respectively, in regions II and IV of the dispersion curve, the graphs of Figs. 20 and 21 exhibit the dynamics of the plane wave in the experimental line. The curves allow us to observe the modulational instability behavior of the signal during its motion in the network as predicted analytically and seen numerically. However, we note that the wave amplitude decreases during the transmission due to dissipation effects induced by the losses of the NLTL. These experimental studies evidence the fact that the NLTL under consideration is a good medium for the propagation of pulse signal voltages.

V. CONCLUSION

In this paper we investigated the influence of the linear capacitance C_S on the characteristic parameters of a modulated wave traveling in the modified Noguchi electrical transmission line by means of the semidiscrete approximation. In the limit of small wave amplitudes, we derived the linear dispersion law and observed that the frequency domain of the carrier wave decreases with the growth of the additional linear dispersive parameter λ. It appears from our study that the bandpass filter under study becomes more selective in terms of the frequency for non-null values of λ.

On the other hand, we considered the semidiscrete approximation and established that the motion of modulated waves in the network is governed by a dispersive nonlinear Schrödinger equation, which differs from the classical NLS equation by the dependence of its coefficients on the additional dispersive capacitance λ. In fact, we have shown that λ has real effects on the dispersion and nonlinear coefficients since its presence has reduced the values of the frequencies for which each of those coefficients is null with related consequences on the instability domains.

Furthermore, we have established that the increment of λ values increases the width of the modulational instability domains that corresponds to $PQ > 0$, while it reduces that of the modulational stability domain, which deals with $PQ < 0$. We also established that the linear dispersive curve is divided into four regions (instead of three, as shown by Marquié *et al.* [6]) owing to the sign of the product PQ and allowing one additional region in the higher-frequency domain for the propagation of the envelope soliton.

For values of the frequency chosen in each zone described by the new dispersion curve (Fig. 10), numerical and experimental simulations carried out on the wave dynamics in the network have led to results that exhibit good agreement with the analytical predictions. This model can be exploited to perform the nerve transmission line exploited by Dikande and Bartholomew [28].

[1] R. Hirota and K. Suzuki, J. Phys. Soc. Jpn. **28**, 1366 (1970).
[2] M. Toda, J. Phys. Soc. Jpn. **23**, 501 (1967).
[3] H. Nagashima and Y. Amagashi, J. Phys. Soc. Jpn. **45**, 680 (1978).
[4] K. Muroya, N. Saitoh, and S. Watanabe, J. Phys. Soc. Jpn. **51**, 1024 (1982).
[5] T. C. Kofane, B. Michaux, and M. Remoissenet, J. Phys. C **21**, 1395 (1988).
[6] P. Marquié, J. M. Bilbault, and M. Remoissenet, Phys. Rev. E **49**, 828 (1994).
[7] F. B. Pelap and T. C. Kofane, Phys. Scr. **57**, 410 (1998).

[8] F. B. Pelap, T. C. Kofane, N. Flytzanis, and M. Remoissenet, J. Phys. Soc. Jpn. **70**, 2568 (2001).
[9] B. Z. Essimbi and I. V. Barashenkov, J. Phys. Soc. Jpn. **71**, 2061 (2002).
[10] E. Kengne, C. Tadmon, and R. Vaillancourt, Chin. J. Phys. **47**, 80 (2009).
[11] F. B. Pelap and M. M. Faye, J. Phys. Soc. Jpn. **76**, 074602 (2007).
[12] M. Remoissenet, *Waves Called Solitons*, 3rd ed. (Springer, Berlin, 1999).
[13] M. Gragoman and D. Jäger, Appl. Phys. Lett. **62**, 110 (1993).
[14] E. Afshari and A. Hajimiri, IEEE J. Solid State Circuits **40**, 744 (2005).
[15] B. Z. Essimbi and D. Jäger, Curr. Appl. Phys. **5**, 567 (2005).
[16] A. Noguchi, Electron. Commun. Jpn. A **57**, 9 (1974).
[17] Y. H. Ichikawa, T. Mitsuhaski, and K. Konno, J. Phys. Soc. Jpn. **41**, 1382 (1976).
[18] T. Yoshinaga and T. Kakutani, J. Phys. Soc. Jpn. **53**, 85 (1984).
[19] F. B. Pelap and M. M. Faye, J. Math. Phys. **46**, 033502 (2005).
[20] E. Kengne and N. Bame, Far East J. Appl. Math. **16**, 213 (2004).
[21] E. Kengne, S. T. Chui, and W. M. Liu, Phys. Rev. E **74**, 036614 (2006).
[22] A. Hirose and K. E. Lonngren, *Introduction to Wave Phenomena* (Wiley Interscience, New York, 1985), p. 329.
[23] T. B. Benjamin and J. E. Feir, J. Fluid Mech. **27**, 417 (1967).
[24] F. Fukushima, M. Wadati, and Y. Narahara, J. Phys. Soc. Jpn. **49**, 1593 (1980).
[25] J. M. Bilbault, P. Marquié, and B. Michaux, Phys. Rev. E **51**, 817 (1995).
[26] P. Marquié, J. M. Bilbault, and M. Remoissenet, Phys. Rev. E **51**, 6127 (1995).
[27] P. Marquié, J. M. Bilbault, and M. Remoissenet, Physica D **87**, 371 (1995).
[28] A. M. Dikande and G. A. Bartholomew, Phys. Rev. E **80**, 041904 (2009).